Inorganic Chemistry

pubs.acs.org/IC

Article

Modulating Excited State Properties and Ligand Ejection Kinetics in Ruthenium Polypyridyl Complexes Designed to Mimic Photochemotherapeutics

Faith N. Robinette, Nathaniel P. Valentine, Konrad M. Sehler, Andrew M. Medeck, Keylon E. Reynolds, Skylar N. Lane, Averie N. Price, Ireland G. Cavanaugh, Steven M. Shell, and Dennis L. Ashford*

Cite This: *Inorg. Chem.* 2024, 63, 8426−8439

Read Online

ACCESS | Metrics & More | Article Recommendations | Supporting Information

ABSTRACT: Ruthenium(II) polypyridyl complexes have gained significant interest as photochemotherapeutics (PCTs) due to their synthetic viability, strong light absorption, well understood excited state properties, and high phototoxicity indexes. Herein, we report the synthesis, characterization, electrochemical, spectrochemical, and preliminary cytotoxicity analyses of three series of ruthenium(II) polypyridyl complexes designed to mimic PCTs. The three series have the general structure of $[Ru(bpy)_2(N{-}N)]^{2+}$ (**Series 1**), $[Ru(bpy)(dmb)(N{-}N)]^{2+}$ (**Series 2**), and $[Ru(dmb)_2(N{-}N)]^{2+}$ (**Series 3**, where N−N is a bidentate polypyridyl ligand, bpy = 2,2′-bipyridine, and dmb = 6,6′-dimethyl-2,2′-bipyridine). In the three series, the N−N ligand was systematically modified to incorporate increased conjugation and/or electronegative heteroatoms to increase dπ-π* backbonding, red-shifting the lowest energy metal-to-ligand charge transfer (MLCT) absorptions from λ_{max} = 454 to λ_{max} = 580 nm, nearing the therapeutic window for PCTs (600−1100 nm). In addition, steric bulk was systematically introduced through the series, distorting the Ru(II) octahedra, making the dissociative ^{3}dd* state thermally accessible at room and body temperatures. This resulted in a 4 orders of magnitude increase in photoinduced ligand ejection kinetics, and demonstrates the ability to modulate both the MLCT* and dd* manifolds in the complexes, which is critical in PCT drug design. Preliminary cell viability assays suggest that the increased steric bulk to lower the ^{3}dd* states may interfere with the cytotoxicity mechanism, limiting photoinitiated toxicity of the complexes. This work demonstrates the importance of understanding both the MLCT* and dd* manifolds and how they impact the ability of a complex to act as a PCT agent.

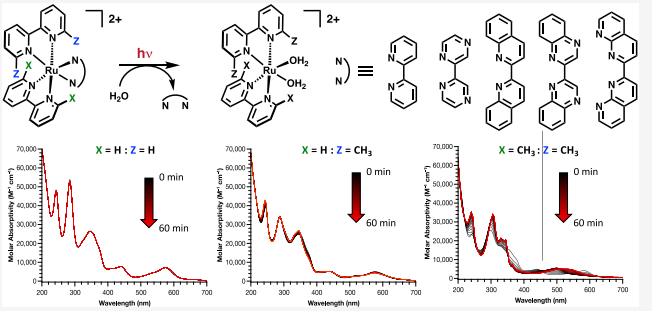

INTRODUCTION

Nearly half of all chemotherapeutics administered today are derived from platinum-based drugs, commonly referred to as platins.[1−3] While these drugs remain widely used, they still suffer from major drawbacks, most notably harsh side-effects due to limited selectivity of malignant cells over healthy ones.[4−9] Photochemotherapy (PCT) and photodynamic therapy (PDT) attempt to overcome these drawbacks by utilizing a compound that is minimally or nontoxic in the dark and in its native state, but becomes cytotoxic under illumination due to a photoinduced reaction. This provides spatiotemporal control of toxicity within the body, ultimately limiting the harsh side-effects associated with traditional platins.[10−13]

PDTs rely on the photoinduced excited state electron transfer (type I) or excited state triplet energy transfer (type II) to generate reactive oxygen species inside the cellular microenvironment, triggering oxidative cell death.[10] While this technique has found use in clinical oncology, the widespread use of PDTs has been limited due to the hypoxic nature of tumor cells and lack of strong light absorption in the near-IR, therapeutic window (600−1100 nm).[14−21] PCTs overcome the limitation of hypoxia in tumorous cells by relying on the photoinduced release of a therapeutic reagent, making them oxygen-independent.[20,22−30] Ru(II) polypyridyl complexes have received significant attention as PCTs due their synthetic viability, relatively long-lived triplet metal-to-ligand charge transfer excited states (^{3}MLCT*), and well understood photophysical behavior.[10,31−40]

Ru(II) PCTs act by either releasing a known cytotoxic reagent from the coordination sphere[23,41−45] or by generating a disolvated activated metal species that can have cisplatin-like

Received: March 5, 2024
Revised: April 10, 2024
Accepted: April 15, 2024
Published: April 25, 2024

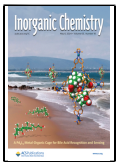

interactions with DNA at the newly opened coordination sites (Figure 1).[22,28,46−48] For successful clinical implementation,

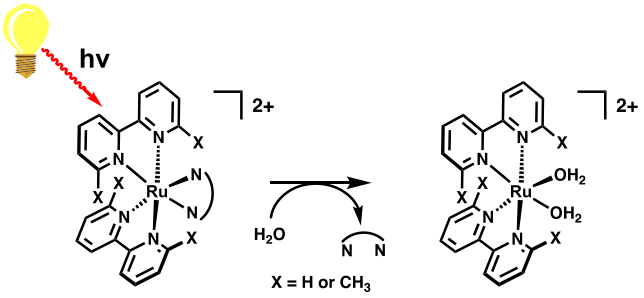

Figure 1. Photoinduced ligand ejection from Ru(II) center to generate disolvated species.

PCTs must absorb light and undergo their photoinduced reactions in the near-IR region, as this light penetrates skin much deeper than blue light due to scattering from biological molecules.[21] While near-IR ligand ejection has been reported for several Ru(II) PCTs, these complexes still have relatively low oscillator strengths at wavelengths >500 nm and typically focus on the ejection of a monodentate ligand as opposed to bidentate ligand ejection required for metalation of DNA.[20,24,29,30,41,46,49−52] Finally, the compounds must be stable in the dark in solution for extended periods and be soluble in biological (aqueous) medium for both clinical viability and photoreactivity with water.

With this in mind, we recently reported a detailed analysis of a series of Ru(II) polypyridyl complexes designed to absorb near the therapeutic window while also introducing steric bulk around the metal center to trigger photoinduced ligand loss.[37] However, we demonstrated that traditional ligand design strategies to red-shift MLCT absorptions by lowering the energy of the π^* orbitals also impacted ligand dissociation kinetics by limiting the accessibility of the dissociative ^{3}dd* states. Photoinduced ligand ejection in Ru(II) octahedral polypyridyl complexes requires thermal population of the formally antibonding ^{3}dd* states from the ^{3}MLCT* excited states.[31,53−55] This is typically achieved by increasing steric bulk around the Ru(II) center, which distorts the pseudo-octahedral, lowering the energy of the ^{3}dd* states. However, if the ^{3}MLCT* state is lowered enough, it can make the thermal barrier (ΔE_{pld}, see Figure 2) to the ^{3}dd* states inaccessible, effectively turning off photoinduced ligand ejection and ultimately the ability of the complex to act as a PCT agent.[37]

Expanding upon this understanding and interplay between the MLCT* manifold energies and dissociative ^{3}dd* states, we set out to design three new series of Ru(II) complexes that allow control over light absorption, thermal stability, photoactivation kinetics, and ultimately photoinduced cytotoxicity. The complexes have the general structure of $[Ru(bpy)_2(N{-}N)]^{2+}$ (**Series 1**), $[Ru(bpy)(dmb)(N{-}N)]^{2+}$ (**Series 2**), and $[Ru(dmb)_2(N{-}N)]^{2+}$ (**Series 3**, where N−N is a bidentate polypyridyl ligand, bpy = 2,2′-bipyridine, and dmb = 6,6′-dimethyl-2,2′-bipyridine, see Figure 3). The N−N ligand was designed to incorporate increased conjugation and/or electronegative heteroatoms within the ligand framework which lowers the energy of ligand π^* orbitals, increasing their π^*-acceptor ability, and resulting in lower MLCT energy absorptions.[31,56−58] Through the series, steric bulk is also systematically introduced by the addition of **dmb** ligands,

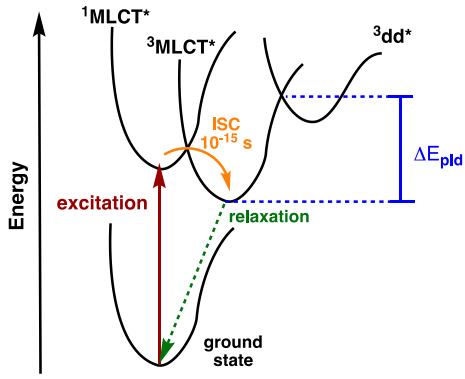

Figure 2. General excited state diagram of Ru(II) polypyridyl complexes showing electronic excitation (red), rapid intersystem crossing (ISC, orange), thermal or electronic relaxation (green), and an activation barrier for photoinduced ligand ejection (ΔE_{pld}).

which distorts the Ru(II) octahedral, making the dissociative ^{3}dd* states more thermally accessible. This demonstrates the importance of understanding ground and excited state energies and how they can impact the ability of a complex to act as a PCT agent. Finally, preliminary cell viability studies suggest additional steric bulk around the Ru(II) metal center and on the photoreleased ligand can inhibit cytotoxic behavior.

RESULTS AND DISCUSSION

Ligand Synthesis. 2,2′-Bipyridine (**bpy**), 6,6′-dimethyl-2,2′-bipyridine (**dmb**), and 2,2′-biquinoline (**bqn**) were purchased form Fischer Scientific and used without further purification. 2,2′-Bipyrizine[59] (**bpz**) and 2,2′-biquinoxaline[37] (**bqx**) were synthesized as previously reported. 2,2′-Bi(1,8-naphthyridine) (**bnn**) was synthesized in 12% yield using a Friedländer condensation of 2-amino-3-formylpyridine and 2,3-butandione in the presence of a base catalyst (Scheme 1). Detailed experimental information is provided in the Supporting Information.

Complex Synthesis. All complex syntheses and manipulations were carried out in the dark to eliminate photoreactions. In addition, all of the complexes were isolated as their chloride salts, which were used for all of the analysis reported herein except for the electrochemical experiments where the complexes were converted to their PF_6 salts via metathesis to avoid chloride interference in the electrochemistry. Purity of the complexes was confirmed by NMR and EA with the data reported in the Supporting Information. It is also important to note that all of the complexes are readily soluble in aqueous media (>200 μM), which is an important aspect for biological applications.

Series 1 complexes were prepared following a previously reported procedure as their chloride salts by the reaction of $Ru(bpy)_2Cl_2$[60] with 1 equiv of the corresponding N−N ligand in 1:1 EtOH/H_2O in a microwave oven reactor at 140 °C for 1 h.[37] The reaction progress of all of the series of complexes was monitored by UV−vis spectroscopy by the disappearance of the $Ru(X)(Y)Cl_2$ (where X and Y are **bpy** or **dmb**) starting material and the appearance of the absorption peaks for the tris-ligated complexes. All complexes were then purified by size exclusion chromatography (Sephadex LH-20 or Sorbadex S-25 fine) using 1:1 H_2O:CH_3OH as eluent, where like fractions, identified by UV−vis, were combined to yield the pure complexes as their chloride salts.

https://doi.org/10.1021/acs.inorgchem.4c00922
Inorg. Chem. 2024, 63, 8426−8439

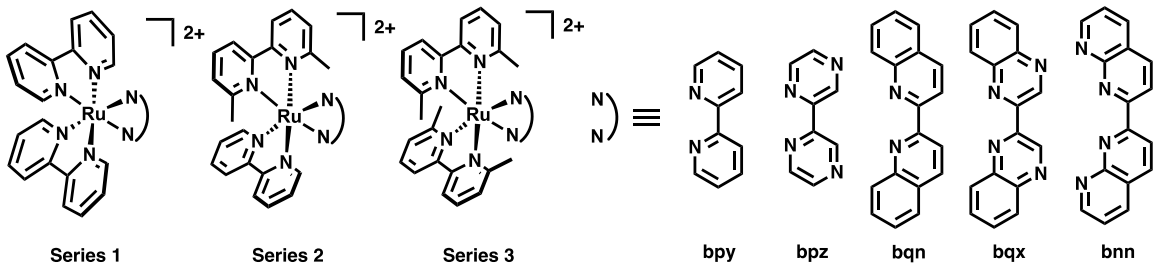

Figure 3. Structures of $[Ru(bpy)_2(N{-}N)]^{2+}$ (**S1**), $[Ru(bpy)(dmb)(N{-}N)]^{2+}$ (**S2**), and $[Ru(dmb)_2(N{-}N)]$ (**S3**) complexes investigated in this study.

Scheme 1. Synthesis of bnn Ligand

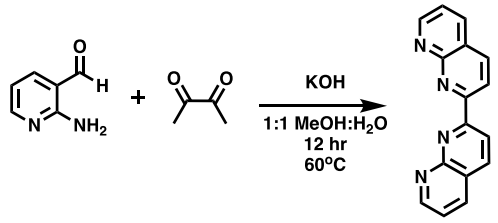

The tris-heteroleptic nature of **Series-2** complexes made their synthesis more challenging and required a step-by-step approach of putting each polypyridyl ligand on the Ru(II) center (Scheme 2). This was achieved by first reacting $[Ru(\eta^6\text{-benzene})(Cl)_2]_2$[61] with 2 equiv of **bpy** in MeOH according to a reported procedure to generate the $[Ru(\eta^6\text{-benzene})(bpy)(Cl)]Cl$ intermediate.[60] The **dmb** ligand was then added by a modified reported procedure[24] in the presence of excess LiCl to prevent the formation of tris-ligated species, giving the $Ru(bpy)(dmb)Cl_2$ intermediate in 66% yield. Finally, the corresponding N−N ligand was then added to the Ru(II) center following the same procedure as that for **Series 1** complexes. To the best of our knowledge, this is one of the most straightforward and high-yielding synthetic preparations for tris-heteroleptic ruthenium compounds reported. Full details are provided in the Supporting Information.

S3-bpy, **S3-bpz**, and **S3-bqn** complexes were synthesized by a slightly modified procedure as that for the **Series 1** complexes. For these complexes, the dichlororuthenium(II) cyclooctadiene polymer[62] was reacted with two equivalents of **dmb** in *o*-dichlorobenzene at 190 °C to generate the $Ru(dmb)_2Cl_2$ intermediate in 71% yield. $Ru(dmb)_2Cl_2$ was then reacted with one equivalent of **bpy**, **bpz**, or **bqn** to generate their respective **Series 3** complexes (Scheme 3). However, this final step did not work with the final two ligands **bqx** and **bnn**. **S3-bnn** was successfully synthesized in 18% yield by reacting $Ru(dmb)_2Cl_2$ with one equivalent of **bnn** in the presence of two equivalents $AgNO_3$ to abstract the chloride ions from the coordination sphere (see Supporting Information for full details). However, despite multiple attempts using a variety of reaction conditions and solvents, **S3-bqx** was not successfully synthesized in quantifiable yields. This suggests that the strong electron-withdrawing nature of the **bqx** ligand, along with the added steric bulk of the two **dmb** ligands, resulted in a relatively unstable complex.

Figure 4 shows representative ^1H NMR data of **S1-bnn**, **S2-bnn**, and **S3-bnn** in D_2O with all NMR data reported in the Supporting Information. Both **S1-bnn** and **S3-bnn** shifts are consistent with C_2 symmetry with corresponding protons in the aromatic region appearing at the same chemical shifts for the **bpy** and **dmb** ligands, respectively. In addition, this symmetry is also observable with the methyl resonances in **S3-bnn** with two equal resonances, one where the attached pyridine ring is opposite the other **dmb** ligand and the other opposite the **bnn** ligand. However, as expected, this symmetry is broken in heteroleptic **S2-bnn** with all aromatic and methyl resonances appearing at different chemical shifts. The aromatic resonances of **S1-bnn** are slightly more deshielded than those of **S2-bnn** and **S3-bnn** due to the electron donating nature of the methyl groups.

Electrochemistry. The electrochemical properties of each complex were analyzed in dry CH_3CN (0.1 M $TBAPF_6$ supporting electrolyte, where $TBAPF_6$ = tetrabutyl ammonium hexafluorophosphate) by cyclic and square-wave voltammetry. It should be noted that each complex was first converted to its PF_6 salt prior to analysis to remove interference from the Cl^- ions (see Supporting Information for details). All of the electrochemical data are reported in Table 1.

All complexes exhibit reversible $[Ru]^{3+/2+}$ redox couples (eq 1) with $E_{1/2}$ values ranging from 1.18 V for **S1-bnn** to 1.64 V for **S2-bqx** (vs SCE). For the same N−N ligand across the series, there is little impact on the $[Ru]^{3+/2+}$ redox potential, demonstrating that the addition of the **dmb** ligands across the series does not significantly impact the Ru(II) $d\pi^6$ energy levels. As an example, the redox potential of the $[Ru]^{3+/2+}$ couple in the **bqn** complexes across the series only varies by 0.05 V, as shown in Figure 5A. The same trend across the series is also observed in the three ligand-based reductions,

Scheme 2. General Synthesis of Heteroleptic S2 Complexes

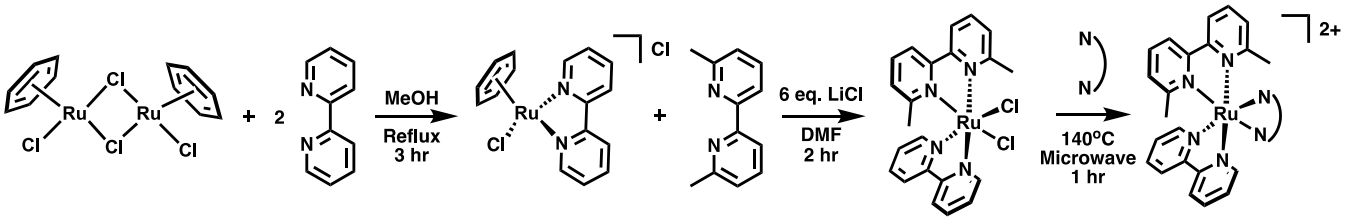

https://doi.org/10.1021/acs.inorgchem.4c00922
Inorg. Chem. 2024, 63, 8426−8439

Scheme 3. General Synthesis of S3 Complexes

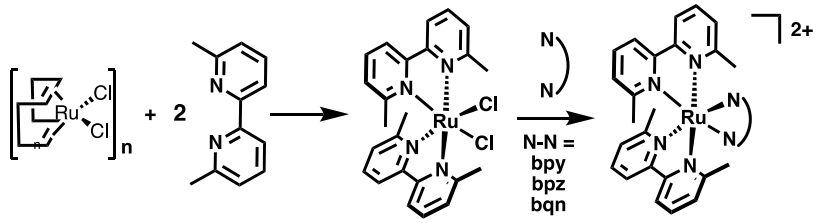

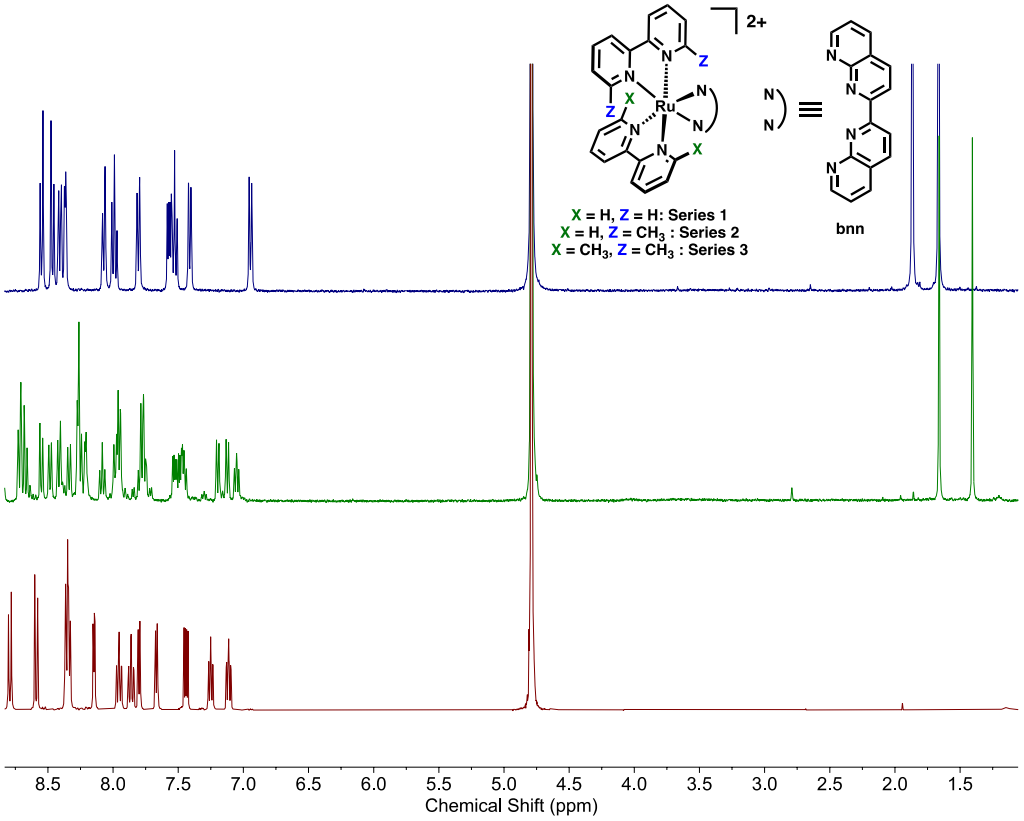

Figure 4. ^{1}H NMR spectra in D_2O at 22 °C of **S1-bnn** (red, bottom), **S2-bnn** (green, middle), and **S3-bnn** (blue, top) at 400 MHz.

where the addition of the **dmb** ligands does not significantly impact reduction potentials. This is demonstrated by all three of the reversible ligand-based reduction potentials for the **bqn** complexes appearing at similar potentials (see Figure 5B and Table 1).

$$[Ru^{III}(bpy)_2(N-N)]^{3+} + e^- \rightarrow [Ru^{II}(bpy)_2(N-N)]^{2+} \quad (1)$$

In contrast, redox potentials within a single series vary significantly as the N−N ligand changes. As an example, the $[Ru]^{3+/2+}$ redox couple in **Series 2** varies from 1.25 V for **S2-bpy** to 1.64 V for **S2-bqx** (vs SCE, see Figure 6A). This shift is due to the increased conjugation and/or addition of electronegative heteroatoms across the N−N ligands. This lowers the energy of the π^* orbitals of the N−N ligand, resulting in increased $d\pi$-π^* backbonding from the Ru(II) center to the N−N ligand, stabilizing the $d\pi^6$ electronic configuration, and ultimately increasing the redox potential for the $[Ru]^{3+/2+}$ couple.[31,64−66] However, the same trend is not observed for the **bnn** ligand across all three series. While the **bnn** ligand has a significant amount of conjugation and electronegative heteroatoms, the additional nitrogens are oriented toward the Ru(II) center as opposed to away from in the case of **bqx**. This allows the additional nitrogens in **bnn** to donate electron density to the Ru(II) center, stabilizing the Ru(III) oxidation state, and lowering the $[Ru]^{3+/2+}$ redox potential (see Figure 6 and Table 1).[67] This is also supported by the fact that for the **bnn** complexes, the $[Ru]^{3+/2+}$ potential increases in the order of **S1-bnn** < **S2-bnn** < **S3-bnn** where the additional methyl groups in **Series 2** and **3** limit the interactions of the extra nitrogens in the **bnn** ligand with the Ru(II) center (see Table 1).

Ligand-based reduction potentials also vary significantly within a series as the N−N bond is changed. Specifically, the variation in the first reduction potential ($[Ru]^{2+/+}$, 0.98 V) is considerably larger than the differences in the second ($[Ru]^{+/0+}$, 0.49 V) and third reduction ($[Ru]^{0/1-}$, 0.16 V) for **Series 2** (see Figure 6 and Table 1). This demonstrates, as expected, that the first reduction is largely N−N ligand centered (eq 2) due to the lower lying π^* orbitals of the N−N ligand, where the second and third reductions occur mainly on the **bpy** and **dmb** ligands of the complexes (eqs 3 and 4).[37] All of the complexes have more positive $[Ru]^{2+/+}$ redox potentials compared to the $[Ru(bpy)_3]^{2+}$ analogs in the series, again due

https://doi.org/10.1021/acs.inorgchem.4c00922
Inorg. Chem. 2024, 63, 8426−8439

Table 1. Electrochemical Properties of all Complexes in N_2 Deaerated CH_3CN (0.1 M $TBAPF_6$ Electrolyte)[a]

compound	$E_{1/2}$ ($[Ru]^{3+/2+}$)	$E_{1/2}$ ($[Ru]^{2+/+}$)	$E_{1/2}$ ($[Ru]^{+/0}$)	$E_{1/2}$ ($[Ru]^{0/1-}$)
S1-bpy	1.29	−1.35	−1.55	−1.78
S1-bpz	1.54	−0.88	−1.44	−1.68
S1-bqn	1.37	−0.92	−1.38	−1.69
S1-bqx	1.60	−0.46	−1.08	−1.61
S1-bnn	1.18	−0.76	−1.24	−1.84
S2-bpy	1.26	−1.39	−1.59	−1.85
S2-bpz	1.54	−0.88	−1.47	−1.70
S2-bqn	1.37	−0.94	−1.46	−1.78
S2-bqx	1.64	−0.46	−1.10	−1.70
S2-bnn	1.23	−0.73	−1.23	−1.86
S3-bpy	1.32	−1.39	−1.64	−1.92
S3-bpz	1.57	−0.85	−1.47	−1.71
S3-bqn	1.42	−0.94	−1.43	−1.84
S3-bnn	1.24	−0.79	−1.32	−2.00

[a]In CH_3CN deaerated with N_2 for 10 min, 1 mM in complex and 0.1 M $TBAPF_6$ supporting electrolyte. The complexes were converted to the PF_6 salt prior to analysis. GC working electrode, graphite rod counter electrode, and $Ag/AgNO_3$ (0.01 M $AgNO_3$ with 0.1 M $TBAPF_6$ in CH_3CN) reference (values were adjusted to agree with literature values for $[Ru(bpy)_3]^{3+/2+}$ at 1.29 V vs SCE).[34,57,63,68] $E_{1/2}$ values from differential pulse voltammetry.

to the lower lying π^*-orbitals of the N−N ligand compared to **bpy** or **dmb**. In general, the more conjugation and/or electronegative heteroatoms on the N−N ligand, the more positive the $[Ru]^{2+/+}$ redox potential due to the lowering of the π^*-orbitals.

$$[Ru^{II}(bpy)(dmb)(N-N)]^{2+} + e^- \rightarrow [Ru^{II}(bpy)(dmb)(N-N^{\bullet-})]^{+} \quad (2)$$

$$[Ru^{II}(bpy)(dmb)(N-N^{\bullet-})]^{+} + e^- \rightarrow [Ru^{II}(bpy^{\bullet-})(dmb)(N-N^{\bullet-})]^{0} \quad (3)$$

$$[Ru^{II}(bpy^{\bullet-})(dmb)(N-N^{\bullet-})]^{0} + e^- \rightarrow [Ru^{II}(bpy^{\bullet-})(dmb^{\bullet-})(N-N^{\bullet-})]^{1-} \quad (4)$$

Unexpectedly, the first reduction potentials of **S1-bnn** and **S2-bnn** are ∼0.3 V more negative than those of the corresponding **S1-bqx** and **S2-bqx** complexes, despite both ligands having the same amount of conjugation and electronegative heteroatoms. The free **bnn** ligand has a slightly more negative reduction potential (−1.44 V vs SCE) compared to the free **bqx** ligand (−1.29 V vs SCE, see Figure S1). In addition, there is likely increased $d\pi$-π^* backbonding from the Ru(II) metal center into the **bnn** ligand compared to the **bqx** ligand given the orientation of the extra nitrogens in **bnn**, resulting in a more negative $[Ru]^{2+/+}$ redox couple. This is supported by the observed lowering of the $[Ru]^{3+/2+}$ redox potential in the **bnn** complexes compared to **bqx** complexes, suggesting significant interactions between the Ru(II) metal center and the four **bnn** nitrogens.

UV−vis Absorption. All of the complexes in water yield intense $\pi \rightarrow \pi^*$ absorption features below 350 nm ($\varepsilon \approx 4.0 \times 10^4$−$7.0 \times 10^4$ M^{-1} cm^{-1}). The complexes that incorporate **bqn**, **bqx**, and **bnn** ligands also feature lower energy and structured absorption transitions between 350−450 nm that are attributed to the $[d\pi^6] \rightarrow [d\pi^5\,\pi_2^*]^1$ transitions of the N−N ligands.[31] All complexes also exhibit broad, lower-energy MLCT bands that range from 400 to 600 nm ($\varepsilon \approx 4.1 \times 10^3$−$4.1 \times 10^3$ M^{-1} cm^{-1}), which as mentioned, is an important feature of moving absorption into the therapeutic window (600−1100 nm) for PCTs. These transitions are assigned as $[d\pi^6] \rightarrow [d\pi^5\,\pi_1^*]^1$ excitations from the Ru(II) metal center to the polypyridyl ligands.[31,55,58,69] Complexes that incorporate the **bpz**, **bqn**, **bqx**, and **bnn** ligands all demonstrate splitting of their MLCT manifolds due to transitions from the Ru(II) center to the **bpy** (or **dmb**, eq 5) ligands and N−N (eq 6) ligand π^*-orbitals for the higher and lower energy transitions, respectively.[31,37]

$$[Ru^{II}(bpy)_2(N-N)]^{2+} + h\nu \rightarrow [Ru^{III}(bpy^{\bullet-})(bpy)(N-N)]^{2+*} \quad (5)$$

$$[Ru^{II}(bpy)_2(N-N)]^{2+} + h\nu \rightarrow [Ru^{III}(bpy)_2(N-N^{\bullet-})]^{2+*} \quad (6)$$

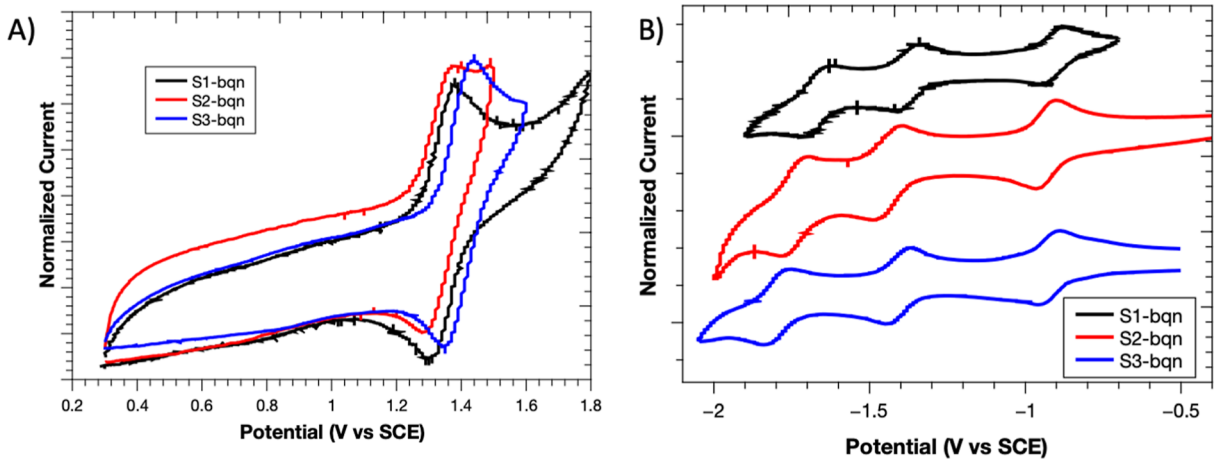

Figure 5. (A) Cyclic voltammograms acquired at 100 mV/s for 1 mM solutions of **S1-bqn**, **S2-bqn**, and **S3-bqn** in N_2 deaerated CH_3CN with 0.1 M $TBAPF_6$ supporting electrolyte. GC working electrode, graphite rod counter electrode, and $Ag/AgNO_3$ reference electrode (0.01 M $AgNO_3$ with 0.1 M $TBAPF_6$ in CH_3CN). Values were adjusted to agree with literature values for $[Ru(bpy)_3]^{3+/2+}$ at 1.29 V vs SCE.[63]

https://doi.org/10.1021/acs.inorgchem.4c00922
Inorg. Chem. 2024, 63, 8426−8439

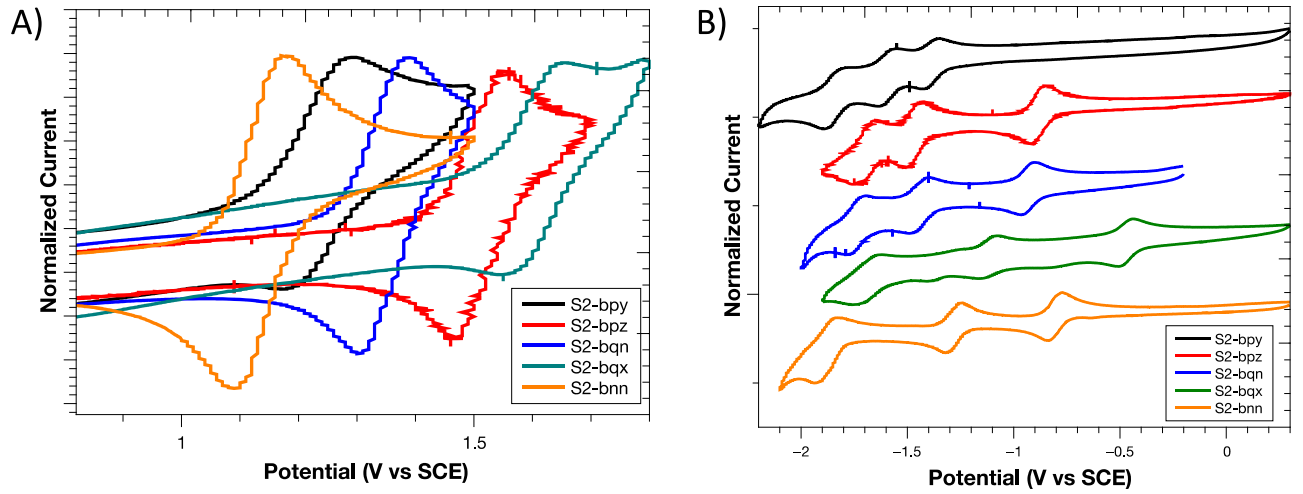

Figure 6. Cyclic voltammograms acquired at 100 mV/s for 1 mM solutions of **S2-bpy, S2-bpz, S2-bqn, S2-bqx**, and **S2-bnn** in N_2 deaerated CH_3CN with 0.1 M $TBAPF_6$ supporting electrolyte. GC working electrode, graphite rod counter electrode, and $Ag/AgNO_3$ reference electrode (0.01 M $AgNO_3$ with 0.1 M $TBAPF_6$ in CH_3CN). Values were adjusted to agree with literature values for $[Ru(bpy)_3]^{3+/2+}$ at 1.29 V vs SCE.[63]

Similar to the electrochemical behavior, through the series for the same N−N ligand, the energies of the MLCT transitions do not shift significantly. This is shown in Figure 7 where the **bnn** complexes only vary from λ_{max} = 578 nm for

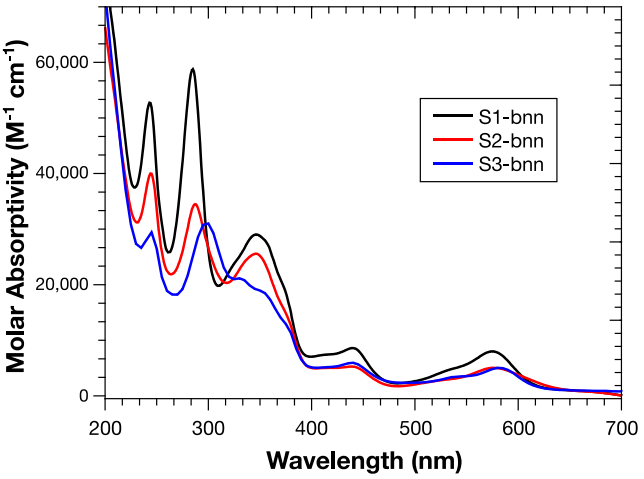

Figure 7. UV−vis spectra of **S1-bnn**, **S2-bnn**, and **S3-bnn** in H_2O at 22 °C.

S1-bnn to λ_{max} = 578 nm for **S3-bnn** (also see Table 2). This suggests that the incorporation of the **dmb** ligands through the series, in addition to the increased steric bulk around the Ru(II) metal center, does not significantly impact the Ru(II) $d\pi^6$ nor the N−N π^*energy states. However, the intensity of the bands does decrease with the addition of **dmb** ligands. This is attributed to slightly weaker coordinative bonds to the Ru(II) center due to the increased steric bulk, resulting in less efficient charge transfer.[70]

In contrast, the energies of the MLCT transitions are significantly altered within a series by varying the N−N ligand through the increase in conjugation and/or introduction of electronegative heteroatoms. These variations lower the energy of the N−N π^*-orbitals, which increases the π^*-acceptor ability of the ligand, resulting in increased $d\pi$-π^* back-bonding.[31,54,69] This results in lower energy MLCT absorption features throughout the series, with the general trend through all series being **bpy** > **bpz** > **bqn** > **bqx** > **bnn**. Figure 8 shows the UV−vis spectra for all of the **Series 2** complexes, with the spectra of all of the complexes shown in Supporting Information, and major features listed in Table 2.

The ground state absorption differences between the complexes that incorporate **bqx** and **bnn** ligands deserve more discussion. For example, **S2-bqx** shows a $\lambda_{max,MLCT}$ = 560 nm with **S2-bnn** being $\lambda_{max,MLCT}$ = 575 nm. Despite both the **bqx** and **bnn** ligands having the same amount of conjugation and electronegative nitrogen atoms, they demonstrate differences in both their electrochemical and their absorption properties. This is because the nitrogens on the **bnn** ligand are oriented toward the Ru(II) center, allowing them to donate electron density, ultimately increasing the energy level of the Ru $d\pi^6$ electron configuration. This results in a less positive oxidation potential for the $Ru^{3+/2+}$ redox couple (see Table 1) for the **bnn** complexes compared to the **bqx** complexes, and also decreases the energy gap between the Ru-$d\pi^6$ and **bnn**-π^* orbitals. As a result, the $[d\pi^6] \rightarrow [d\pi^5\ \pi_1^*]^1$ MLCT absorption feature for the **bnn** ligand complexes are lower in energy throughout the series (Table 2).

Photoinduced Ligand Ejection. A key aspect of the PCT phototoxicity mechanism is the loss of a bidentate ligand under illumination to trigger DNA-metalation and ultimately apotosis.[22,48,71,72] We previously reported and discussed the critical interplay between therapeutic window absorption and photoinduced ligand ejection.[37] The series reported herein extends this work by moving the MLCT absorptions near the therapeutic window, while also systematically introducing steric bulk around the Ru(II) metal center to modulate photoinduced ligand ejection kinetics. The rate constant for photoinduced ligand dissociation (k_{pld}) was measured at both 22 and 37 °C (average body temperature) using the apparatus shown in Figure S5. The UV−vis spectra of each complex were taken at known time intervals during illumination with white light to determine k_{pld} (see Supporting Information for full details).

Representative UV−vis spectra of **S1-bnn**, **S2-bnn**, and **S3-bnn** under illumination at 37 °C are shown in Figure 9 with all of the spectra shown in the Supporting Information (Figures S6−S8). As shown in Figures 9 and S6−S8, there is a strong dependence on both the steric bulk around the Ru(II) metal

https://doi.org/10.1021/acs.inorgchem.4c00922
Inorg. Chem. 2024, 63, 8426−8439

Table 2. Spectroscopic and Photoinduced Ligand Ejection Properties for all Complexes

compound	absorbance λ (nm) (ε, $\times 10^3$ M^{-1} cm^{-1})[a]	k_{pld} (s^{-1})[b]@ 22°C	k_{pld} (s^{-1})[b]@ 37°C	k_{pld} λ fit (nm)[c]
S1-bpy	454 (11.6)			
	417 (8.7)			
	286 (69.9)			
S1-bpz	486 (7.3)			
	406 (8.5)			
	281 (47.2)			
S1-bqn	527 (5.6)	4.5×10^{-5}	5.2×10^{-5}	527[d]
	440 (5.8)			
	287 (40.6)			
S1-bqx	563 (5.9)			
	405 (16.7)			
	383 (17.4)			
	285 (41.2)			
S1-bnn	575 (7.4)			
	440 (8.0)			
	349 (26.9)			
	285 (54.6)			
S2-bpy	455 (11.9)	7.0×10^{-3}	7.3×10^{-3}	457
	425 (8.7)			
	285 (67.9)			
S2-bpz	485 (9.5)			
	410 (11.1)			
	285 (56.7)			
S2-bqn	526 (6.7)	5.3×10^{-3}	1.1×10^{-2}	379
	440 (4.9)			
	291 (34.5)			
S2-bqx	560 (7.6)			
	405 (21.2)			
	385 (22.0)			
	275 (39.2)			
S2-bnn	575 (8.7)		$<10^{-5}$	582
	440 (9.7)			
	346 (29.8)			
	285 (57.4)			
S3-bpy	460 (10.1)	2.2×10^{-3}	2.8×10^{-3}	460
	428 (7.6)			
	295 (48.1)			
S3-bpz	500 (9.3)	9.5×10^{-4}	2.2×10^{-3}	415
	415 (11.6)			
	290 (43.0)			
S3-bqn	520 (6.7)	1.9×10^{-3}	1.7×10^{-3}	356[e]
	440 (6.7)			
	300 (45.4)			
S3-bnn	580 (4.1)	5.0×10^{-3}	6.4×10^{-3}	580
	440 (5.5)			
	325 (19.2)			
	300 (29.1)			

[a]Measured in H_2O. [b]Measured in H_2O monitored over time during irradiation with light from a GLORIOUS-LITE 30 W LED (240 W halogen equivalent, 3000 LM, broad spectrum) placed 5 cm above the sample while stirring (see Figure S5). [c]Wavelength chosen for kinetic fits to reduce the interferences from the photoproduct absorption and maximize sensitivity of the measurement (highest ε). [d]Fit over the full-hour photolysis due to the reaction being much slower. [e]Note this was the best wavelength to monitor despite significant overlap between the starting material and photoproduct.

center (**Series 1** → **Series 3**) and the amount of conjugation and/or electronegative heteroatoms on the N−N ligand on the

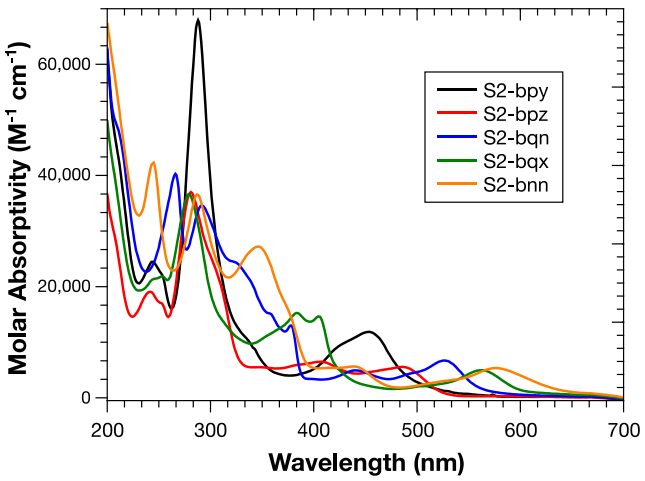

Figure 8. UV−vis absorption spectra of **S2-bpy, S2-bpz, S2-bqn, S2-bqx**, and **S2-bnn** in H_2O at 22 °C.

extent and rate of photoinduced ligand ejection. A brief summary of all of the spectra reveal; (1) for **Series 1**, only the **S1-bqn** complex shows measurable photodissociation, (2) in **Series 2** the **S2-bpy** and **S2-bqn** complex show complete dissociation in 60 s with **S2-bnn** showing minor dissociation at 37 °C, and (3) all **Series 3** complexes demonstrate measurable dissociation at 22 and 37 °C (see Table 2 and Figures S6−S8). In addition, all complexes (except **S3-bqn**) have a faster k_{pld} at higher temperatures. **S3-bqn** repeatedly showed slightly slower kinetics at elevated temperatures suggesting the reaction was near barrierless at the temperatures studied herein or the differences in rates were within the experimental error. It should also be noted that all of the complexes showed no dissociation in water and no or minor dissociation in the cell culture medium for at least 30 days (Figure S12).

In general and as expected, the rate of photoinduced ligand dissociation increases through the series for the same N−N ligand as the steric bulk around the Ru(II) center increases. For example, **S1-bnn** shows no observable ligand ejection over the hour-long photolysis, **S2-bnn** undergoes minimal ligand ejection over the hour, where **S3-bnn** shows complete ligand ejection in less than 60 s (Figure 9). The increased steric bulk in **S3-bnn** lowers the energy of the formally antibonding ^{3}dd* state, making it thermally accessible at the temperatures analyzed (see Figure 2). A more detailed description of the kinetics and excited state processes will be presented in the next section. Analysis of the spectra of **S3-bnn** under irradiation shows a decrease in intensity of the $[d\pi^6] \rightarrow [d\pi^5 \pi_1^*(bnn)]^1$ MLCT transition at 580 nm as well a decrease in the $[d\pi^6] \rightarrow [d\pi^5 \pi_2^*(bnn)]^1$ transitions around 380 nm. The resulting spectrum for **S3-bnn**, as well as all of the other compounds that undergo photoinduced ligand ejection, are similar to those reported for diaquated ruthenium(II) complexes.[22,37,73−75] This suggest ejection of one of the bulkier N−N or **dmb** ligands from the coordination sphere under irradiation (eq 7).[37]

$$[Ru^{II}(bpy)_2(N-N)]^{2+} + h\nu \rightarrow [Ru^{II}(bpy)_2(OH_2)_2]^{2+} + N-N \quad (7)$$

Photolyzed samples of **S1-bqn**, **S2-bqn** and **S3-bqn** were subjected to high-resolution electrospray mass spectrometry in an attempt to fully characterize the photoproducts. Analysis of

https://doi.org/10.1021/acs.inorgchem.4c00922
Inorg. Chem. 2024, 63, 8426−8439

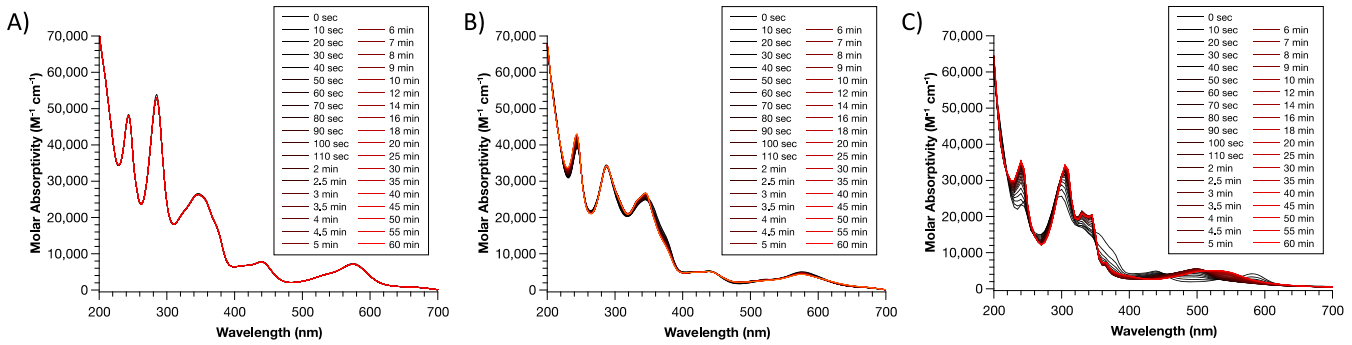

Figure 9. Absorption spectra of complexes **S1-bnn** (A), **S2-bnn** (B), and **S3-bnn** (C) in 3 mL H_2O at 37 °C monitored over time during irradiation with light from a GLORIOUS-LITE 30 W LED (240 W halogen equivalent, 3000 LM, broad spectrum) placed 5 cm above the sample (see Figure S5).

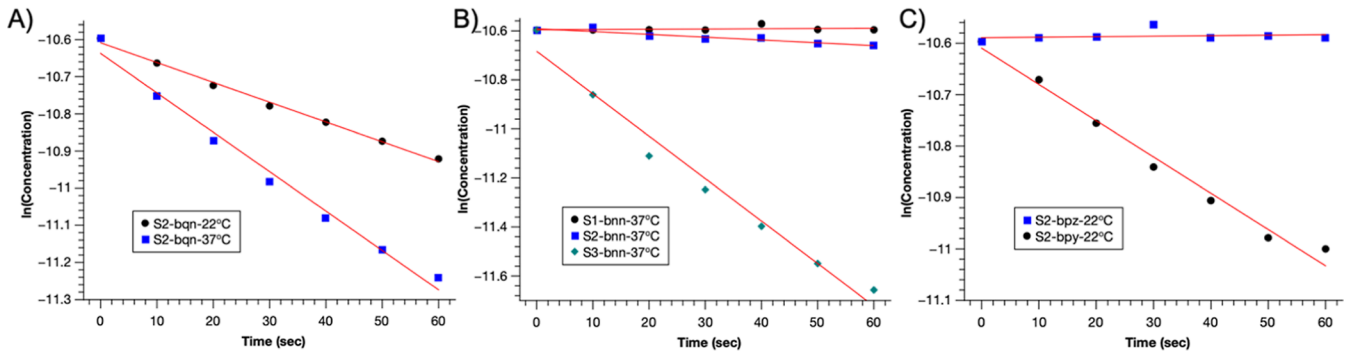

Figure 10. First-order fits (red lines) for photoinduced ligand dissociation of ln(concentration) versus time for **S2-bqn** at 22 and 37 °C (A), **S1-bnn**, **S2-bnn**, and **S3-bnn** at 37 °C (B), and **S2-bpy** and **S2-bpz** at 22 °C (C).

the **S1-bqn** spectra shows a signal at m/z = 257.1068, corresponding to the protonated photoejected **bqn** ligand and no evidence of free **bpy** (see Figure S11). Spectra of **S2-bqn** and **S3-bqn** photolyzed samples display both a signal at m/z = 257.1069 as well as a larger one at m/z = 185.1071, corresponding to the protonated photoejected **dmb** ligand. This demonstrates that for the **Series 2** and **3** complexes, both the **dmb** and N−N ligand are able to be photoejected from the coordination sphere. Attempts to characterize the ruthenium species following illumination proved to be more challenging using this method. This is possibly due to continued photoreaction of the diaquated species, such as the formation of neutral, high-valent, ruthenium oxo species from the Ru(II)-aqua photoproducts, under extended photolysis conditions.[75,76] This is supported by the appearance of $[Ru^{IV}(bpy)_2(OH)_2]^{2+}$ (m/z = 448.0460) in the photolysis sample of **S1-bqn** and $[Ru^{VI}(bpy)(dmb)(O)_2]^{2+}$ (m/z = 474.0619) in the photolysis sample of **S2-bqn** (see Figure S11). Future studies will focus on fully characterizing the ruthenium species throughout the photolysis period to better understand speciation during illumination.

The kinetics for photoinduced ligand ejection were fit to a first order reaction equation for all of the complexes that underwent quantifiable ligand dissociation with rate constants (k_{pld}) reported in Table 2 at 22 and 37 °C and representative fits shown in Figure 10 (all fits are shown in the Supporting Information). In general and as expected, k_{pld} increases with increasing temperature. For example, k_{pld} for **S2-bqn** is 5.3 × 10^{-3} and 1.1 × 10^{-2} s^{-1} at 22 and 37 °C, respectively (see Figure 10A). Also, as expected, k_{pld} generally increases across the series from **Series 1** to **Series 3** (see Figure 10B). As an example, **S1-bnn** shows no observable photoinduced ligand ejection, with **S2-bnn** having $k_{pld} < 10^{-5}$ s^{-1} (the small changes in the spectra made quantifying k_{pld} not possible) and **S3-bnn** k_{pld} = 6.4 × 10^{-3} s^{-1} at 37 °C. This is due to increased steric bulk around the Ru(II) center distorting the pseudo-octahedral, lowering the energy of the formally antibonding ^{3}dd* states and making them thermally accessible from the ^{3}MLCT* excited states.[31,53−55]

However, steric bulk and the energies of the ^{3}dd* states are not the only considerations for ligand ejection kinetics, as ^{3}MLCT* excited-state energies also play a critical role.[37] As an example, **S2-bpy** undergoes complete ligand ejection within 60 s under these conditions with k_{pld} = 4.5 × 10^{-3} s^{-1} at 22 °C. However, **S2-bpz**, despite having little to no difference sterically, and thus similar ^{3}dd* energies, shows no measurable photoreaction under the same conditions (see Figure 10C and Table 2). The **bpz** ligand has lower lying π*-orbitals due to the extra electronegative nitrogen atoms compared to those of **bpy**. This lowers the energy of ^{3}MLCT* excited state, increasing the activation energy barrier (ΔE_{pld}, energy gap for photoinduced ligand dissociation, see Figure 2) between the ^{3}MLCT* and ^{3}dd* states, making them inaccessible at these temperatures.[37] A more detailed description of this phenomenon is presented in the next section.

Unexpectedly, both **S3-bpy** and **S3-bqn** demonstrated slightly lower k_{pld} values compared to those of **S2-bpy** and **S2-bqn**. This could be attributed to the ^{3}MLCT* → ^{3}dd* electron transfer moving into the Marcus inverted region, lowering k_{pld} despite having a larger free energy loss in the photoreaction.[34] However, more experimentation is needed to

https://doi.org/10.1021/acs.inorgchem.4c00922
Inorg. Chem. 2024, 63, 8426−8439

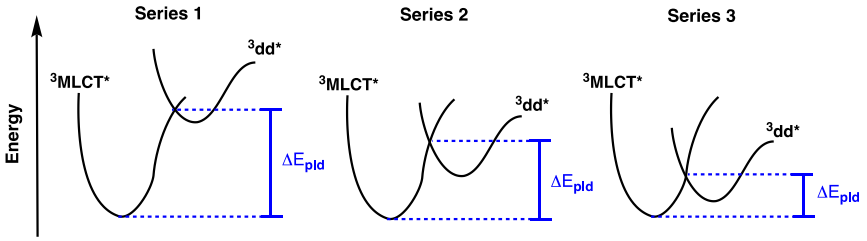

Figure 11. Representative excited state diagrams of the ruthenium polypyridyl complexes through the series with the same N−N ligand. Note the relative energy of the ^{3}MLCT* state does not change, but there is a lowering of the ^{3}dd* state through increased steric bulk.

confirm this hypothesis and is outside the scope of the present study.

Controlling Photoinduced Ligand Dissociation. The demands on clinically used PCTs are high, including high thermal stability in the dark in both the solid form and in solution, facile ligand ejection kinetics under illumination, aqueous solubility, and high cytotoxicity activity upon illumination. Due to these demands, the aim of this study was to not only move the MLCT absorptions near and into the therapeutic window but also control photoinduced ligand ejection kinetics while balancing thermal stability. This has been achieved through the series described herein by carefully controlling both the MLCT manifolds, the ^{3}dd* state energies, and ultimately the activation energy (ΔE_{pld}) between these two states.

Upon initial photoexcitation into the ^{1}MLCT* excited state, the complexes rapidly undergo intersystem crossing into a ^{3}MLCT* state, which can then relax back to the ground state or thermally populate the formally antibonding metal-centered ^{3}dd* state (sometimes referred to as the ^{3}MC state), triggering ligand dissociation (see Figure 2). Note that the extent of thermal relaxation into the ^{3}MLCT* state is expected to be similar across the series.[37] The final electron transfer into the ^{3}dd* state can be described as a $d\pi^5 d\pi^{*1} \rightarrow d\pi^5 d\sigma^{*1}$ transition.[54,55,77−79] Ligand ejection from the ^{3}dd* state is rapid compared to relaxation back to the MLCT manifold and/or ground state.[54,58,80,81] Through the series with the same N−N ligand, k_{pld} increases significantly with increasing steric bulk. For example, k_{pld} increases at least 4 orders of magnitude through the series for the **bnn** ligand in the order **S1-bnn** ($\ll 10^{-6}$ s^{-1}) < **S2-bnn** ($<10^{-5}$ s^{-1}) < **S3-bnn** (6.4×10^{-3} s^{-1}) at 37 °C. As discussed above, this is due to distorting the pseudo-octahedral, lowering the ^{3}dd* states and making them thermally accessible (decreasing ΔE_{pld}) from the ^{3}MLCT* excited states (Figure 11).[31,53−55] Note that the ^{3}MLCT* energies do not change significantly through the series for the same N−N ligand, as supported by both the electrochemical and absorption data.

A similar phenomenon is also observed within a series for varying N−N ligands and the accessibility of the ^{3}dd* states. However, in this case, the steric considerations and therefore the ^{3}dd* state energy levels stay relatively the same, but the MLCT* manifolds shift with varying ligands. For instance, **S2-bqn** has $k_{pld} = 1.1 \times 10^{-2}$ s^{-1} at 37 °C where **S2-bqx** shows no observable photodissociation. While both complexes have the same steric bulk around the Ru(II) metal center, the additional nitrogens on the **bqx** ligand lowers the energy of the MLCT manifolds by ∼0.14 eV, increasing the activation energy (ΔE_{pld}) into the dissociative ^{3}dd* state, and shutting off photodissociation at these temperatures (Figure 12).

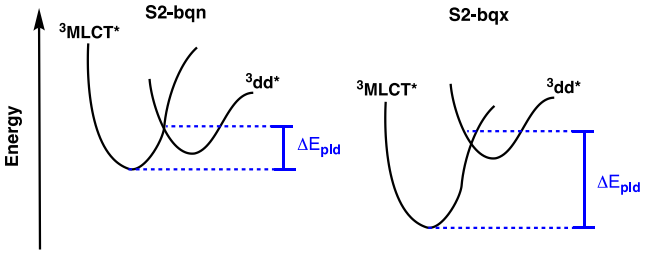

Figure 12. Representative excited state diagrams of the ruthenium polypyridyl complexes through the series with varying N−N ligand. Note that the relative energy of the ^{3}dd* state does not change, but lowering of the ^{3}MLCT* manifold through introduction of electronegative heteroatoms and/or conjugation.

Cytotoxicity Assays. Preliminary MTT (3-[4,5-dimethylthiazol-2-yl]-2,5 diphenyl tetrazolium bromide) dye reduction assays were used to analyze the potential biological activity of all of the complexes against human embryonic kidney (HEK293T) cell cultures with and without illumination. Briefly, HEK293T were seeded into 96-well plates and dosed with varying concentrations of the complexes. The cultures were then either exposed to white light for 10 min or covered from irradiation in situ (see Supporting Information for full experimental details). All of the cell viability assays for each complex in the dark and under illumination are shown in Figure S12 and summarized in Table S1. Figure 13 shows representative data of each complex at 100 μM with and without illumination.

Analysis of the cell viability data shows that all of the complexes reported herein are minimally toxic in the dark and in their native state. In addition, as expected, complexes that do not undergo facile photoinduced ligand ejection do not show increased toxicity under illumination. However, unexpectedly, not all of the complexes that undergo facile photoinduced ligand ejection demonstrated toxicity under illumination. Control experiments with cisplatin and etoposide did not show light dependence on toxicity, suggesting that illumination alone would not trigger cell death.

Only **S2-bpy** (PTI = 3.9), **S3-bpy** (PTI = 1.6), **S2-bqn** (PTI = 2.4), and **S3-bqn** (PTI = 3.1) showed a statistically significant photoinduced toxicity index (PTI, ratio of $IC_{50,dark}$ over $IC_{50,light}$, see Table S1). **S2-bpy** showed the highest PTI of all of the complexes, although our measured PTI's are significantly lower than those reported for the same complex on HL60 leukemia (PTI = 188) and A549 lung (PTI = 136) cancer cells by Glazer and co-workers.[22] The PTIs observed for the complexes reported herein are also lower than other recently reported Ru(II) PCTs such as the Ru(II) cytochrome P450 3A4 inhibitor reported by Toupin et al. (PTI = 9),[82] a trisheteroleptic Ru(II) complex that inhibited conjunctival

https://doi.org/10.1021/acs.inorgchem.4c00922
Inorg. Chem. 2024, 63, 8426−8439

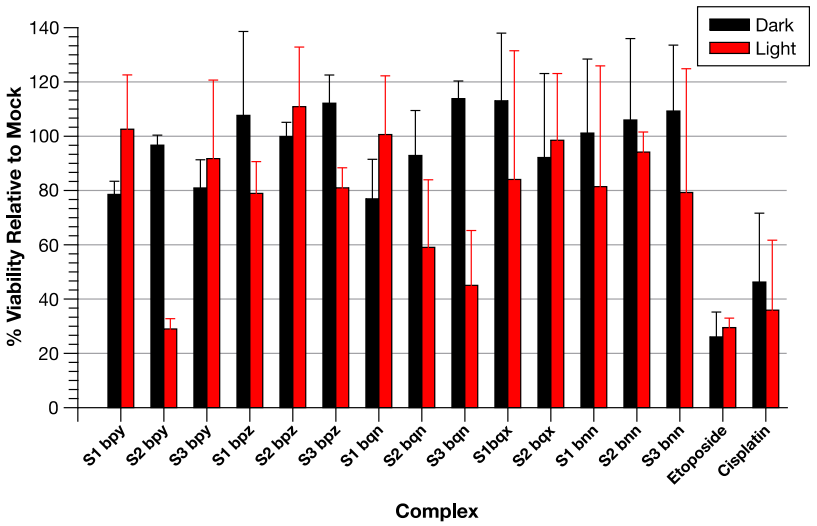

Figure 13. Percent change in HEK293T cell viability of 100 μM of each complex either illuminated with a GLORIOUS-LITE 30 W LED (240 W halogen equivalent, 3000 LM, broad spectrum) placed 10 cm above the sample (light, red bars) or covered in situ from illumination (dark, black bars). Etoposide and cisplatin (20 μM) were included as positive controls.

melanoma growth in zebrafish reported by Chen et al. (PTI = 31),[83] and $[Ru(bpy)_2(pz)_2]^{2+}$ derivatives (where pz = pyrazole) against A549 cells reported by Hirahara et al. (PTI = 7.3).[84] However, a direct comparison between PTIs is difficult given the wide range of experimental variables including cell line, growth medium, irradiation source, distance, flux, and time. This is demonstrated by the lowered PTIs for **S2-bpy** in our experiment compared to the conditions used by Glazer and co-workers.

In an effort to elucidate the cytotoxicity mechanism of the complexes with the highest PTI's, Western blot and immunofluorescence microscopy experiments were completed. Histone H2AX phosphorylation mediated by the ATR/ATM kinase cascade is a common marker of damaged DNA in cells.[85−87] H2AX phosphorylation was analyzed by Western blot as a function of treatment with cisplatin, **S1−S3 bpy, bqn**, and **bnn** complexes under irradiation. As shown in Figure S14, H2AX phosphorylation is relatively low in mock-treated cells but increases upon the addition of cisplatin. Incubation of cells with the Ru(II) complexes following irradiation resulted in increases in H2AX phosphorylation relative to mock treatment, with the **S3-bqn** sample resulting in the highest level of phosphorylation. In addition, immunofluorescence microscopy was used to investigate the histone phosphorylation phenotype for cells treated with the compounds that showed the highest PTIs. Treatment of the cells with cisplatin, **S2-bpy**, **S2-bqn**, and **S3-bqn** resulted in formation of distinct nuclear foci of H2AX phosphorylation, indicative of DNA damage centers (Figure S15). Taken together, these results suggest that the compounds with the highest PTIs cause DNA damage under irradiation, which likely contributes to their cytotoxic effects.

Interestingly, **S2-bpy** demonstrated a 2.4× increase in PTI compared to **S3-bpy**, despite both complexes showing complete ligand dissociation in less than 1 min under illumination. This suggests that the additional steric bulk in the photoproducts, both the Ru(II)-diaquated species and the ejected ligand, can inhibit toxicity and ultimately PCT behavior. This is supported by the fact that majority of the complexes that exhibit facile photoinduced ligand ejection due to increased steric bulk around the Ru(II) center (**Series 2** and **Series 3**) do not show significant increased toxicity under illumination. In addition, the smallest metal photoproduct likely released in all of the complexes is $[Ru(bpy)_2(OH_2)_2]^{2+}$ from the **S2-bpy** complex, which resulted in the highest PTI in this study.[22] This suggests that the diaquated-Ru(II) metal center needs to be relatively unobstructed to interact with the DNA base pairs, which leads to cellular apopotosis.[22,28] Finally, both **S2-bqn** and **S3-bqn** show increased toxicity under illumination where the other complexes with similar k_{pld} do not, suggesting the **bqn** ligand may act as a DNA intercalator causing cell death. Further studies are needed to better understand the cytotoxic behavior of these complexes and to determine why the bulkier complexes may be inhibited within the cellular microenvironment. While these data demonstrate that addition of steric bulk around the Ru(II) metal center facilitates photoinduced ligand ejection, it may also lead to inhibited PCT behavior.

CONCLUSIONS

We have described here the synthesis, characterization, electrochemical, spectrochemical, and preliminary cytotoxicity analyses of three series of ruthenium(II) polypyridyl complexes designed to mimic PCTs. The complexes were designed to incorporate increased conjugation and/or electronegative heteroatoms within the ligand frameworks to lower the ligand π^* orbitals and move absorptions near the therapeutic window. The lowest energy MLCT absorption maximum was red-shifted from λ_{max} = 454 nm for **S1-bpy** to λ_{max} = 580 nm for **S3-bnn**. In addition, steric bulk was also systematically introduced throughout the series by the incorporation of **dmb** ligands, distorting the Ru(II) octahedral structure and making the dissociative ^{3}dd* state thermally accessible at room and body temperature. Photoinduced ligand ejection kinetics increased by at least 4 orders of magnitude throughout the series. Furthermore, the incorporation of the sterically bulky **dmb** ligands did not significantly alter the ground state or excited state manifolds involved in redox chemistry and light absorption. These findings are important in understanding the ground and excited state energies with respect to PCT agents. However, it appears that the addition of steric bulk around the Ru(II) metal center inhibits the cytotoxic behavior of the

https://doi.org/10.1021/acs.inorgchem.4c00922
Inorg. Chem. 2024, 63, 8426−8439

photoproducts, ultimately limiting the PCT activity of these complexes.

■ ASSOCIATED CONTENT

Supporting Information

The Supporting Information is available free of charge at https://pubs.acs.org/doi/10.1021/acs.inorgchem.4c00922.

Experimental and synthetic procedures, characterization data of complexes, UV−visible spectra of all complexes, experimental photolysis setup, photolysis data and kinetic traces for all complexes at 22 and 37 °C, ESI-MS of photolysis samples, complex stability in DMEM cell culture medium, cell viability assays, western blot analysis, and immunofluorescence microscopy of selected complexes (PDF)

■ AUTHOR INFORMATION

Corresponding Author

Dennis L. Ashford − *Department of Natural Sciences, Tusculum University, Greeneville, Greeneville, Tennessee 37745, United States;* orcid.org/0000-0002-2931-6063; Email: dashford@tusculum.edu

Authors

Faith N. Robinette − *Department of Natural Sciences, Tusculum University, Greeneville, Greeneville, Tennessee 37745, United States*

Nathaniel P. Valentine − *Department of Natural Sciences, Tusculum University, Greeneville, Greeneville, Tennessee 37745, United States*

Konrad M. Sehler − *Department of Natural Sciences, Tusculum University, Greeneville, Greeneville, Tennessee 37745, United States*

Andrew M. Medeck − *Department of Natural Sciences, Tusculum University, Greeneville, Greeneville, Tennessee 37745, United States*

Keylon E. Reynolds − *Department of Natural Sciences, Tusculum University, Greeneville, Greeneville, Tennessee 37745, United States*

Skylar N. Lane − *Department of Natural Sciences, Tusculum University, Greeneville, Greeneville, Tennessee 37745, United States*

Averie N. Price − *Department of Natural Sciences, Tusculum University, Greeneville, Greeneville, Tennessee 37745, United States*

Ireland G. Cavanaugh − *Department of Natural Sciences, Tusculum University, Greeneville, Greeneville, Tennessee 37745, United States*

Steven M. Shell − *Department of Natural Sciences, University of Virginia College at Wise, Wise, Virginia 24293, United States*

Complete contact information is available at: https://pubs.acs.org/10.1021/acs.inorgchem.4c00922

Notes

The authors declare no competing financial interest.

■ ACKNOWLEDGMENTS

This work was supported by the Arthur Vining Davis Foundations under grant no. G-2206-23043 and Eastman Chemical Company supporting F.N.B, N.P.V., K.M.S., A.M.M., K.E.R., S.N.L., A.N.P., I.G.C., and D.L.A. Cytotoxicity analysis was carried out by S.M.S. at the University of Virginia College at Wise. Mass spectrometric analyses were performed at the University of Tennessee, Knoxville Biological and Small Molecule Mass Spectrometry Core with the assistance of Nick Trybala, Dr. Hector F. Castro, and Vernon Stafford.

■ REFERENCES

(1) Siegel, R. L.; Miller, K. D.; Jemal, A. Cancer statistics, 2020. *CA A Cancer J. Clin.* **2020**, *70* (1), 7−30.

(2) Atlanta: American Cancer Society, Inc Global Cancer Facts & Figures, 4th ed, 2024. https://www.cancer.org/content/dam/cancer-org/research/cancer-facts-and-statistics/global-cancer-facts-and-figures/global-cancer-facts-and-figures-2024.pdf (accessed Sep 23, 2021).

(3) Paprocka, R.; Wiese-Szadkowska, M.; Janciauskiene, S.; Kosmalski, T.; Kulik, M.; Helmin-Basa, A. Latest developments in metal complexes as anticancer agents. *Coord. Chem. Rev.* **2022**, *452*, 214307.

(4) Galanski, M.; Jakupec, M. A.; Keppler, B. K. Update of the preclinical situation of anticancer platinum complexes: novel design strategies and innovative analytical approaches. *Curr. Med. Chem.* **2005**, *12* (18), 2075−2094.

(5) Johnstone, T. C.; Park, G. Y.; Lippard, S. J. Understanding and improving platinum anticancer drugs—phenanthriplatin. *Anticancer Res.* **2014**, *34* (1), 471−476.

(6) Mistry, P.; Kelland, L. R.; Abel, G.; Sidhar, S.; Harrap, K. R. The relationships between glutathione, glutathione-S-transferase and cytotoxicity of platinum drugs and melphalan in eight human ovarian carcinoma cell lines. *Br. J. Cancer* **1991**, *64* (2), 215−220.

(7) Kelland, L. The resurgence of platinum-based cancer chemotherapy. *Nat. Rev. Cancer* **2007**, *7* (8), 573−584.

(8) Yang, P.; Ebbert, J. O.; Sun, Z.; Weinshilboum, R. M. Role of the glutathione metabolic pathway in lung cancer treatment and prognosis: a review. *J. Clin. Oncol.* **2006**, *24* (11), 1761−1769.

(9) Shi, J.; Kantoff, P. W.; Wooster, R.; Farokhzad, O. C. Cancer nanomedicine: progress, challenges and opportunities. *Nat. Rev. Cancer* **2017**, *17* (1), 20−37.

(10) Monro, S.; Colón, K. L.; Yin, H.; Roque, J.; Konda, P.; Gujar, S.; Thummel, R. P.; Lilge, L.; Cameron, C. G.; McFarland, S. A. Transition metal complexes and photodynamic therapy from a tumor-centered approach: challenges, opportunities, and highlights from the development of TLD1433. *Chem. Rev.* **2019**, *119* (2), 797−828.

(11) Imberti, C.; Zhang, P.; Huang, H.; Sadler, P. J. New designs for phototherapeutic transition metal complexes. *Angew. Chem., Int. Ed. Engl.* **2020**, *59* (1), 61−73.

(12) Heinemann, F.; Karges, J.; Gasser, G. Critical overview of the use of Ru(II) polypyridyl complexes as photosensitizers in one-photon and two-photon photodynamic therapy. *Acc. Chem. Res.* **2017**, *50* (11), 2727−2736.

(13) Zhang, Y.; Zhou, Q.; Tian, N.; Li, C.; Wang, X. Ru(II)-complex-based DNA photocleaver having intense absorption in the phototherapeutic window. *Inorg. Chem.* **2017**, *56* (4), 1865−1873.

(14) Jarvi, M. T.; Patterson, M. S.; Wilson, B. C. Insights into photodynamic therapy dosimetry: simultaneous singlet oxygen luminescence and photosensitizer photobleaching measurements. *Biophys. J.* **2012**, *102* (3), 661−671.

(15) Clement, S.; Deng, W.; Camilleri, E.; Wilson, B. C.; Goldys, E. M. X-ray induced singlet oxygen generation by nanoparticle-photosensitizer conjugates for photodynamic therapy: determination of singlet oxygen quantum yield. *Sci. Rep.* **2016**, *6* (1), 19954.

(16) Weersink, R. A.; Bogaards, A.; Gertner, M.; Davidson, S. R. H.; Zhang, K.; Netchev, G.; Trachtenberg, J.; Wilson, B. C. Techniques for delivery and monitoring of TOOKAD (WST09)-mediated photodynamic therapy of the prostate: clinical experience and practicalities. *J. Photochem. Photobiol. B Biol.* **2005**, *79* (3), 211−222.

(17) Kohler, L.; Nease, L.; Vo, P.; Garofolo, J.; Heidary, D. K.; Thummel, R. P.; Glazer, E. C. Photochemical and photobiological activity of Ru(II) homoleptic and heteroleptic complexes containing

methylated bipyridyl-type ligands. *Inorg. Chem.* **2017**, *56* (20), 12214−12223.
(18) Griffith, C.; Dayoub, A. S.; Jaranatne, T.; Alatrash, N.; Mohamedi, A.; Abayan, K.; Breitbach, Z. S.; Armstrong, D. W.; MacDonnell, F. M. Cellular and cell-free studies of catalytic DNA cleavage by ruthenium polypyridyl complexes containing redox-active intercalating ligands. *Chem. Sci.* **2017**, *8* (5), 3726−3740.
(19) Yadav, A.; Janaratne, T.; Krishnan, A.; Singhal, S. S.; Yadav, S.; Dayoub, A. S.; Hawkins, D. L.; Awasthi, S.; MacDonnell, F. M. Regression of lung cancer by hypoxia-sensitizing ruthenium polypyridyl complexes. *Mol. Cancer Ther.* **2013**, *12* (5), 643−653.
(20) Steinke, S. J.; Gupta, S.; Piechota, E. J.; Moore, C. E.; Kodanko, J. J.; Turro, C. Photocytotoxicity and photoinduced phosphine ligand exchange in a Ru(II) polypyridyl complex. *Chem. Sci.* **2022**, *13* (7), 1933−1945.
(21) König, K. Multiphoton microscopy in life sciences. *J. Microsc.* **2000**, *200* (2), 83−104.
(22) Howerton, B. S.; Heidary, D. K.; Glazer, E. C. Strained ruthenium complexes are potent light-activated anticancer agents. *J. Am. Chem. Soc.* **2012**, *134* (20), 8324−8327.
(23) Arora, K.; Herroon, M.; Al-Afyouni, M. H.; Toupin, N. P.; Rohrabaugh, T. N.; Loftus, L. M.; Podgorski, I.; Turro, C.; Kodanko, J. J. Catch and release photosensitizers: combining dual-action ruthenium complexes with protease inactivation for targeting invasive cancers. *J. Am. Chem. Soc.* **2018**, *140* (43), 14367−14380.
(24) Al-Afyouni, M. H.; Rohrabaugh, T. N.; Al-Afyouni, K. F.; Turro, C. New Ru(II) photocages operative with near-IR light: new platform for drug delivery in the PDT window. *Chem. Sci.* **2018**, *9* (32), 6711−6720.
(25) Havrylyuk, D.; Heidary, D. K.; Sun, Y.; Parkin, S.; Glazer, E. C. Photochemical and photobiological properties of pyridyl-pyrazol(in)-e-based ruthenium(II) complexes with sub-micromolar cytotoxicity for phototherapy. *ACS Omega* **2020**, *5* (30), 18894−18906.
(26) Shi, H.; Imberti, C.; Sadler, P. J. Diazido platinum(IV) complexes for photoactivated anticancer chemotherapy. *Inorg. Chem. Front.* **2019**, *6* (7), 1623−1638.
(27) van Rixel, V. H. S.; Ramu, V.; Auyeung, A. B.; Beztsinna, N.; Leger, D. Y.; Lameijer, L. N.; Hilt, S. T.; Le Dévédec, S. E.; Yildiz, T.; Betancourt, T.; Gildner, M. B.; Hudnall, T. W.; Sol, V.; Liagre, B.; Kornienko, A.; Bonnet, S. Photo-uncaging of a microtubule-targeted rigidin analogue in hypoxic cancer cells and in a xenograft mouse model. *J. Am. Chem. Soc.* **2019**, *141* (46), 18444−18454.
(28) Hachey, A. C.; Havrylyuk, D.; Glazer, E. C. Biological activities of polypyridyl-type ligands: implications for bioinorganic chemistry and light-activated metal complexes. *Curr. Opin. Chem. Biol.* **2021**, *61*, 191−202.
(29) Roque, J. A., III; Cole, H. D.; Barrett, P. C.; Lifshits, L. M.; Hodges, R. O.; Kim, S.; Deep, G.; Frances-Monerris, A.; Alberto, M. E.; Cameron, C. G.; McFarland, S. A. Intraligand excited states turn a ruthenium oligothiophene complex into a light-triggered ubertoxin with anticancer effects in extreme hypoxia. *J. Am. Chem. Soc.* **2022**, *144* (18), 8317−8336.
(30) Cole, H. D.; Roque, J. A.; Shi, G.; Lifshits, L. M.; Ramasamy, E.; Barrett, P. C.; Hodges, R. O.; Cameron, C. G.; McFarland, S. A. Anticancer agent with inexplicable potency in extreme hypoxia: characterizing a light-triggered ruthenium ubertoxin. *J. Am. Chem. Soc.* **2022**, *144* (22), 9543−9547.
(31) Ashford, D. L.; Glasson, C. R. K.; Norris, M. R.; Concepcion, J. J.; Keinan, S.; Brennaman, M. K.; Templeton, J. L.; Meyer, T. J. Controlling ground and excited state properties through ligand changes in ruthenium polypyridyl complexes. *Inorg. Chem.* **2014**, *53* (11), 5637−5646.
(32) Reichardt, C.; Monro, S.; Sobotta, F. H.; Colón, K. L.; Sainuddin, T.; Stephenson, M.; Sampson, E.; Roque, J.; Yin, H.; Brendel, J. C.; Cameron, C. G.; McFarland, S.; Dietzek, B. Predictive strength of photophysical measurements for in vitro photobiological activity in a series of Ru(II) polypyridyl complexes derived from π-extended ligands. *Inorg. Chem.* **2019**, *58* (5), 3156−3166.
(33) Fong, J.; Kasimova, K.; Arenas, Y.; Kaspler, P.; Lazic, S.; Mandel, A.; Lilge, L. A novel class of ruthenium-based photosensitizers effectively kills in vitro cancer cells and in vivo tumors. *Photochem. Photobiol. Sci.* **2015**, *14* (11), 2014−2023.
(34) Thompson, D. W.; Ito, A.; Meyer, T. J. $[Ru(bpy)_3]^{2+*}$ and other remarkable metal-to-ligand charge transfer (MLCT) excited states. *Pure Appl. Chem.* **2013**, *85* (7), 1257−1305.
(35) Demas, J. N.; Adamson, A. W. Tris (2,2′-bipyridine)ruthenium-(II) sensitized reactions of some oxalato complexes. *J. Am. Chem. Soc.* **1973**, *95* (16), 5159−5168.
(36) Bock, C. R.; Meyer, T. J.; Whitten, D. G. Electron transfer quenching of the luminescent excited state of tris(2,2′-bipyridine)-ruthenium(II). Flash photolysis relaxation technique for measuring the rates of very rapid electron transfer reactions. *J. Am. Chem. Soc.* **1974**, *96* (14), 4710−4712.
(37) McCullough, A. B.; Chen, J.; Valentine, N. P.; Franklin, T. M.; Cantrell, A. P.; Darnell, V. M.; Qureshi, Q.; Hanson, K.; Shell, S. M.; Ashford, D. L. Balancing the interplay between ligand ejection and therapeutic window light absorption in ruthenium polypyridyl complexes. *Dalton Trans.* **2022**, *51* (26), 10186−10197.
(38) Chettri, A.; Yang, T.; Cole, H. D.; Shi, G.; Cameron, C. G.; McFarland, S. A.; Dietzek-Ivansic, B. Using biological photophysics to map the excited-state topology of molecular photosensitizers for photodynamic therapy. *Angew. Chem., Int. Ed.* **2023**, *62* (17), No. e202301452.
(39) Ankathatti Munegowda, M.; Manalac, A.; Weersink, M.; McFarland, S. A.; Lilge, L. Ru(II) containing photosensitizers for photodynamic therapy: a critique on reporting and an attempt to compare efficacy. *Coord. Chem. Rev.* **2022**, *470*, 214712.
(40) Bonnet, S. Ruthenium-based photoactivated chemotherapy. *J. Am. Chem. Soc.* **2023**, *145* (43), 23397−23415.
(41) Lameijer, L. N.; Ernst, D.; Hopkins, S. L.; Meijer, M. S.; Askes, S. H. C.; Le Dévédec, S. E.; Bonnet, S. A red-light-activated ruthenium-caged NAMPT inhibitor remains phototoxic in hypoxic cancer cells. *Angew. Chem. Int. Ed.* **2017**, *56* (38), 11549−11553.
(42) Respondek, T.; Garner, R. N.; Herroon, M. K.; Podgorski, I.; Turro, C.; Kodanko, J. J. Light activation of a cysteine protease inhibitor: caging of a peptidomimetic nitrile with $Ru^{II}(bpy)_2$. *J. Am. Chem. Soc.* **2011**, *133* (43), 17164−17167.
(43) Zamora, A.; Denning, C. A.; Heidary, D. K.; Wachter, E.; Nease, L. A.; Ruiz, J.; Glazer, E. C. Ruthenium-containing P450 inhibitors for dual enzyme inhibition and DNA damage. *Dalton Trans.* **2017**, *46* (7), 2165−2173.
(44) Karges, J.; Heinemann, F.; Jakubaszek, M.; Maschietto, F.; Subecz, C.; Dotou, M.; Vinck, R.; Blacque, O.; Tharaud, M.; Goud, B.; Viñuelas Zahínos, E.; Spingler, B.; Ciofini, I.; Gasser, G. Rationally designed long-wavelength absorbing Ru(II) polypyridyl complexes as photosensitizers for photodynamic therapy. *J. Am. Chem. Soc.* **2020**, *142* (14), 6578−6587.
(45) Li, A.; Yadav, R.; White, J. K.; Herroon, M. K.; Callahan, B. P.; Podgorski, I.; Turro, C.; Scott, E. E.; Kodanko, J. J. Illuminating cytochrome P450 binding: Ru(ii)-caged inhibitors of CYP17A1. *Chem. Commun.* **2017**, *53* (26), 3673−3676.
(46) Cole, H. D.; Roque, J. A., 3rd; Lifshits, L. M.; Hodges, R.; Barrett, P. C.; Havrylyuk, D.; Heidary, D.; Ramasamy, E.; Cameron, C. G.; Glazer, E. C.; McFarland, S. A. Fine-feature modifications to strained ruthenium complexes radically alter their hypoxic anticancer activity. *Photochem. Photobiol.* **2022**, *98* (1), 73−84.
(47) Wachter, E.; Zamora, A.; Heidary, D. K.; Ruiz, J.; Glazer, E. C. Geometry matters: inverse cytotoxic relationship for cis/trans-Ru(ii) polypyridyl complexes from cis/trans-$[PtCl_2(NH_3)_2]$. *Chem. Commun.* **2016**, *52* (66), 10121−10124.
(48) Wachter, E.; Heidary, D. K.; Howerton, B. S.; Parkin, S.; Glazer, E. C. Light-activated ruthenium complexes photobind DNA and are cytotoxic in the photodynamic therapy window. *Chem. Commun.* **2012**, *48* (77), 9649−9651.
(49) Loftus, L. M.; Al-Afyouni, K. F.; Turro, C. New Ru(II) scaffold for photoinduced ligand release with red light in the photodynamic therapy (PDT) window. *Chem.—Eur. J.* **2018**, *24*, 11550−11553.

https://doi.org/10.1021/acs.inorgchem.4c00922
Inorg. Chem. 2024, 63, 8426−8439

(50) Meijer, M. S.; Natile, M. M.; Bonnet, S. 796 nm activation of a photocleavable ruthenium(II) complex conjugated to an upconverting nanoparticle through two phosphonate groups. *Inorg. Chem.* **2020**, *59* (20), 14807−14818.
(51) Steinke, S. J.; Piechota, E. J.; Loftus, L. M.; Turro, C. Acetonitrile ligand photosubstitution in Ru(II) complexes directly from the 3MLCT state. *J. Am. Chem. Soc.* **2022**, *144* (44), 20177−20182.
(52) Havrylyuk, D.; Hachey, A. C.; Fenton, A.; Heidary, D. K.; Glazer, E. C. Ru(II) photocages enable precise control over enzyme activity with red light. *Nat. Commun.* **2022**, *13* (1), 3636.
(53) Knoll, J. D.; Albani, B. A.; Turro, C. Excited state investigation of a new Ru(II) complex for dual reactivity with low energy light. *Chem. Commun.* **2015**, *51* (42), 8777−8780.
(54) Caspar, J. V.; Meyer, T. J. Photochemistry of MLCT excited states. Effect of nonchromophoric ligand variations on photophysical properties in the series cis-Ru(bpy)2L22+. *Inorg. Chem.* **1983**, *22* (17), 2444−2453.
(55) Durham, B.; Caspar, J. V.; Nagle, J. K.; Meyer, T. J. Photochemistry of tris(2,2′-bipyridine)ruthenium(2+) ion. *J. Am. Chem. Soc.* **1982**, *104* (18), 4803−4810.
(56) Anderson, P. A.; Strouse, G. F.; Treadway, J. A.; Keene, F. R.; Meyer, T. J. Black MLCT absorbers. *Inorg. Chem.* **1994**, *33* (18), 3863−3864.
(57) Anderson, P. A.; Richard Keene, F.; Meyer, T. J.; Moss, J. A.; Strouse, G. F.; Treadway, J. A. Manipulating the properties of MLCT excited states. *J. Chem. Soc., Dalton Trans.* **2002**, No. 20, 3820−3831.
(58) Caspar, J. V.; Meyer, T. J. Photochemistry of tris(2,2′-bipyridine)ruthenium(2+) ion (Ru(bpy)32+). Solvent effects. *J. Am. Chem. Soc.* **1983**, *105* (17), 5583−5590.
(59) Schultz, D. M.; Sawicki, J. W.; Yoon, T. P. An improved procedure for the preparation of $Ru(bpz)_3(PF_6)_2$ via a high-yielding synthesis of 2,2′-bipyrazine. *Beilstein J. Org. Chem.* **2015**, *11*, 61−65.
(60) Norris, M. R.; Concepcion, J. J.; Glasson, C. R. K.; Fang, Z.; Lapides, A. M.; Ashford, D. L.; Templeton, J. L.; Meyer, T. J. Synthesis of phosphonic acid-derivatized bipyridine ligands and their ruthenium complexes. *Inorg. Chem.* **2013**, *52* (21), 12492−12501.
(61) Bennett, M. A.; Smith, A. K. Arene ruthenium(II) complexes formed by dehydrogenation of cyclohexadienes with ruthenium(III) trichloride. *J. Chem. Soc., Dalton Trans.* **1974**, No. 2, 233−241.
(62) Doi, T.; Nagamiya, H.; Kokubo, M.; Hirabayashi, K.; Takahashi, T. Synthesis of a tetrabenzyl-substituted 10-membered cyclic diamide. *Tetrahedron* **2002**, *58* (15), 2957−2963.
(63) Lever, A. B. P. Electrochemical parametrization of metal complex redox potentials, using the ruthenium(III)/ruthenium(II) couple to generate a ligand electrochemical series. *Inorg. Chem.* **1990**, *29* (6), 1271−1285.
(64) Yam, V. W.-W.; Lee, V. W.-M.; Ke, F.; Siu, K.-W. M. Synthesis, photophysics, and electrochemistry of ruthenium(II) polypyridine complexes with crown ether pendants. *Inorg. Chem.* **1997**, *36* (10), 2124−2129.
(65) Rillema, D. P.; Mack, K. B. The low-lying excited state in ligand .pi.-donor complexes of ruthenium(II): mononuclear and binuclear species. *Inorg. Chem.* **1982**, *21* (10), 3849−3854.
(66) Ackermann, M. N.; Interrante, L. V. Ruthenium(II) complexes of modified 1,10-phenanthrolines. 1. Synthesis and properties of complexes containing dipyridophenazines and a dicyanomethylene-substituted 1,10-phenanthroline. *Inorg. Chem.* **1984**, *23* (24), 3904−3911.
(67) Thummel, R. P.; Lefoulon, F.; Chirayil, S. A ruthenium tris(diimine) complex with three different ligands. *Inorg. Chem.* **1987**, *26* (18), 3072−3074.
(68) Gu, J.; Chen, J.; Schmehl, R. H. Using intramolecular energy transfer to transform non-photoactive, visible-light-absorbing chromophores into sensitizers for photoredox reactions. *J. Am. Chem. Soc.* **2010**, *132* (21), 7338−7346.
(69) Caspar, J. V.; Kober, E. M.; Sullivan, B. P.; Meyer, T. J. Application of the energy gap law to the decay of charge-transfer excited states. *J. Am. Chem. Soc.* **1982**, *104* (2), 630−632.
(70) Thummel, R. P.; Lefoulon, F. Polyaza cavity shaped molecules. 11. Ruthenium complexes of annelated 2,2′-biquinoline and 2,2′-bi-1,8-naphthyridine. *Inorg. Chem.* **1987**, *26* (5), 675−680.
(71) White, J. K.; Schmehl, R. H.; Turro, C. An overview of photosubstitution reactions of Ru(II) imine complexes and their application in photobiology and photodynamic therapy. *Inorg. Chim. Acta* **2017**, *454*, 7−20.
(72) Singh, T. N.; Turro, C. Photoinitiated DNA Binding by cis-$[Ru(bpy)_2(NH_3)_2]^{2+}$. *Inorg. Chem.* **2004**, *43* (23), 7260−7262.
(73) Durham, B.; Wilson, S. R.; Hodgson, D. J.; Meyer, T. J. Cis-trans photoisomerization in $Ru(bpy)_2(OH_2)_2^{2+}$. Crystal structure of trans-$[Ru(bpy)_2(OH_2)(OH)](ClO_4)_2$. *J. Am. Chem. Soc.* **1980**, *102* (2), 600−607.
(74) Gama Sauaia, M. l.; Tfouni, E.; Helena de Almeida Santos, R.; Teresa do Prado Gambardella, M.; Del Lama, M. P. F. M.; Fernando Guimarães, L.; Santana da Silva, R. Use of HPLC in the identification of cis and trans-diaquabis(2,2′-bipyridine)ruthenium(II) complexes: crystal structure of cis-$[Ru(H_2O)_2(bpy)_2](PF_6)_2$. *Inorg. Chem. Commun.* **2003**, *6* (7), 864−868.
(75) Paul, L.; Enkhbold, K.; Robinson, S.; Aye, T. T.; Chung, Y.; Harrison, D. P.; Pollock, J. A.; Norris, M. R. Unravelling the role of $[Ru(bpy)_2(OH_2)_2]^{2+}$ complexes in photo-activated chemotherapy. *J. Inorg. Biochem.* **2022**, *235*, 111930.
(76) Dovletoglou, A.; Meyer, T. J. Mechanism of cis-directed four-electron oxidation by a trans-dioxo complex of ruthenium(VI). *J. Am. Chem. Soc.* **1994**, *116* (1), 215−223.
(77) Baranoff, E.; Collin, J. P.; Furusho, J.; Furusho, Y.; Laemmel, A. C.; Sauvage, J. P. Photochemical or thermal chelate exchange in the ruthenium coordination sphere of complexes of the Ru(phen)(2)L family (L = diimine or dinitrile ligands). *Inorg. Chem.* **2002**, *41* (5), 1215−1222.
(78) Mobian, P.; Kern, J. M.; Sauvage, J. P. Light-driven machine prototypes based on dissociative excited states: photoinduced decoordination and thermal recoordination of a ring in a ruthenium-(II)-containing [2]catenane. *Angew. Chem., Int. Ed. Engl.* **2004**, *43* (18), 2392−2395.
(79) Sun, Q.; Mosquera-Vazquez, S.; Suffren, Y.; Hankache, J.; Amstutz, N.; Lawson Daku, L. M.; Vauthey, E.; Hauser, A. On the role of ligand-field states for the photophysical properties of ruthenium(II) polypyridyl complexes. *Coord. Chem. Rev.* **2015**, *282*−*283*, 87−99.
(80) Sun, Q.; Mosquera-Vazquez, S.; Lawson Daku, L. M.; Guénée, L.; Goodwin, H. A.; Vauthey, E.; Hauser, A. Experimental evidence of ultrafast quenching of the 3MLCT luminescence in ruthenium(II) tris-bipyridyl complexes via a 3dd state. *J. Am. Chem. Soc.* **2013**, *135* (37), 13660−13663.
(81) Thompson, D. W.; Fleming, C. N.; Myron, B. D.; Meyer, T. J. Rigid medium stabilization of metal-to-ligand charge transfer excited states. *J. Phys. Chem. B* **2007**, *111* (24), 6930−6941.
(82) Toupin, N.; Steinke, S. J.; Nadella, S.; Li, A.; Rohrabaugh, T. N., Jr.; Samuels, E. R.; Turro, C.; Sevrioukova, I. F.; Kodanko, J. J. Photosensitive Ru(II) complexes as inhibitors of the major human drug metabolizing enzyme CYP3A4. *J. Am. Chem. Soc.* **2021**, *143* (24), 9191−9205.
(83) Chen, Q.; Cuello-Garibo, J.-A.; Bretin, L.; Zhang, L.; Ramu, V.; Aydar, Y.; Batsiun, Y.; Bronkhorst, S.; Husiev, Y.; Beztsinna, N.; Chen, L.; Zhou, X.-Q.; Schmidt, C.; Ott, I.; Jager, M. J.; Brouwer, A. M.; Snaar-Jagalska, B. E.; Bonnet, S. Photosubstitution in a trisheteroleptic ruthenium complex inhibits conjunctival melanoma growth in a zebrafish orthotopic xenograft model. *Chem. Sci.* **2022**, *13* (23), 6899−6919.
(84) Hirahara, M.; Iwamoto, A.; Teraoka, Y.; Mizuno, Y.; Umemura, Y.; Uekita, T. Ruthenium pyrazole complexes: a family of highly active metallodrugs for photoactivated chemotherapy. *Inorg. Chem.* **2024**, *63* (4), 1988−1996.
(85) Ray, A.; Blevins, C.; Wani, G.; Wani, A. A. ATR- and ATM-mediated DNA damage response is dependent on excision repair assembly during G1 but not in S phase of cell cycle. *PLoS One* **2016**, *11* (7), No. e0159344.

https://doi.org/10.1021/acs.inorgchem.4c00922
Inorg. Chem. 2024, 63, 8426−8439

(86) Redon, C.; Pilch, D.; Rogakou, E.; Sedelnikova, O.; Newrock, K.; Bonner, W. Histone H2A variants H2AX and H2AZ. *Curr. Opin. Genet. Dev.* **2002**, *12* (2), 162−169.
(87) Solier, S.; Sordet, O.; Kohn, K. W.; Pommier, Y. Death receptor-induced activation of the Chk2- and histone H2AX-associated DNA damage response pathways. *Mol. Cell. Biol.* **2009**, *29* (1), 68−82.

https://doi.org/10.1021/acs.inorgchem.4c00922
Inorg. Chem. 2024, 63, 8426−8439